# Composition of low-lying $J=\frac{3}{2}^\pm$ Δ-baryons

Langtian Liu (刘浪天)[,][1,2] Chen Chen (陈晨)[,][3,4,*] Ya Lu (陆亚),[1,2,5] Craig D. Roberts[,][1,2,†] and Jorge Segovia[ ][6,2]

[1]*School of Physics, Nanjing University, Nanjing, Jiangsu 210093, China*
[2]*Institute for Nonperturbative Physics, Nanjing University, Nanjing, Jiangsu 210093, China*
[3]*Interdisciplinary Center for Theoretical Study, University of Science and Technology of China,
Hefei, Anhui 230026, China*
[4]*Peng Huanwu Center for Fundamental Theory, Hefei, Anhui 230026, China*
[5]*Department of Physics, Nanjing Tech University, Nanjing 211816, China*
[6]*Departamento Sistemas Físicos, Químicos y Naturales, Universidad Pablo de Olavide, E-41013 Sevilla, Spain*

A Poincaré-covariant quark + diquark Faddeev equation is used to develop insights into the structure of the four lightest $(I, J^P = \frac{3}{2}, \frac{3}{2}^\pm)$ baryon multiplets. While these systems can contain isovector-axialvector and isovector-vector diquarks, one may neglect the latter and still arrive at a reliable description. The $(\frac{3}{2}, \frac{3}{2}^+)$ states are the simpler systems, with features that bear some resemblance to quark model pictures, e.g., their most prominent rest-frame orbital angular momentum component is S-wave and the $\Delta(1600)\frac{3}{2}^+$ may reasonably be viewed as a radial excitation of the $\Delta(1232)\frac{3}{2}^+$. The $(\frac{3}{2}, \frac{3}{2}^-)$ states are more complex: the $\Delta(1940)\frac{3}{2}^-$ expresses little of the character of a radial excitation of the $\Delta(1700)\frac{3}{2}^-$; and while the rest-frame wave function of the latter is predominantly P-wave, the leading piece in the $\Delta(1940)\frac{3}{2}^-$ wave function is S-wave, in conflict with quark model expectations. Experiments that can test these predictions, such as large momentum transfer resonance electroexcitation, may shed light on the nature of emergent hadron mass.

I. INTRODUCTION

Questions relating to the composition of baryons have been asked for roughly one hundred years. Answers possessing an appealing simplicity within the framework of quantum mechanics were provided by the (constituent) quark model [1] via its progeny, *viz.* three-body potential models [2–6]. In such models, baryons constituted from combinations of up (u), down (d), and strange (s) valence quark flavors can be grouped into multiplets of SU(6) ⊗ O(3), labeled by their flavor content, spin, and orbital angular momentum. From this perspective, the four lightest $(I, J^P = \frac{3}{2}, \frac{3}{2}^\pm)$ Δ-baryons, built from isospin $I = \frac{3}{2}$ combinations of three u and/or d quarks, are viewed as follows: $\Delta(1232)\frac{3}{2}^+$, S-wave ground-state; $\Delta(1600)\frac{3}{2}^+$, radial excitation of the $\Delta(1232)$, hence, S-wave; $\Delta(1700)\frac{3}{2}^-$, $L = 1$ orbital angular momentum excitation

of the $\Delta(1232)$, so, P-wave; and $\Delta(1940)\frac{3}{2}^-$, radial excitation of the $\Delta(1700)$, thus, also P-wave.

Quark models are practically useful in many applications; yet, so far as spectra are concerned, they typically produce masses for radial excitations of the ground-state that are too large when compared with the lowest-mass orbital angular momentum excitation [[7], Sec. 15]. The best known example is the Roper resonance, $N(1440)\frac{1}{2}^+$, discussed elsewhere [8], which is predicted to lie above the nucleon's parity partner, $N(1535)\frac{1}{2}^-$, in contradiction of experiment. The same issue is encountered in decuplet baryons with, e.g., the calculated mass of the $\Delta(1600)\frac{3}{2}^+$ being greater than that of the $\Delta(1700)\frac{3}{2}^-$.

Potential models are also challenged by quantum chromodynamics (QCD), which requires a Poincaré covariant description of baryon structure that leads to a Poincaré invariant explanation of their properties [9]. For instance, the evaluation of hadron distribution functions (DFs) requires Poincaré covariance in order to ensure, *inter alia*, the proper domain of DF support [10]; and modern electroproduction experiments are probing ground- and excited-state baryons using photons with virtuality approaching $10m_p^2$ [11–13], where m_p is the proton mass. Furthermore, while the total angular momentum of a bound-state is Poincaré-invariant, this is not true of any
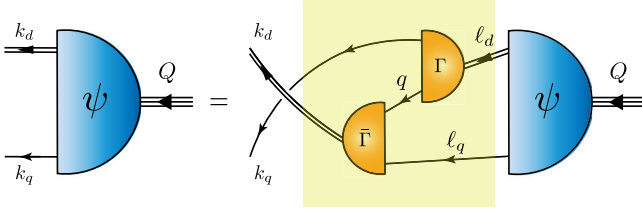
*chenchen1031@ustc.edu.cn
†cdroberts@nju.edu.cn

FIG. 1. Quark + diquark Faddeev equation, a linear integral equation for the Poincaré-covariant matrix-valued function ψ, the Faddeev amplitude for a baryon with total momentum $Q = \ell_q + \ell_d = k_q + k_d$. ψ describes the relative momentum correlation between the dressed-quarks and -diquarks. Legend. Shaded rectangle—Faddeev kernel; single line—dressed-quark propagator, $S(\ell)$; $\Gamma^{J^P}(k; K)$—diquark correlation amplitude; and double line—diquark propagator, $D^{J^P}(K)$.
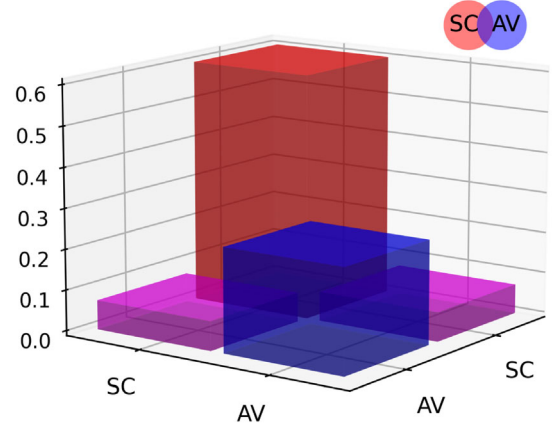

FIG. 2. Contributions of the various diquark components to the canonical normalization of the Poincaré-covariant nucleon Faddeev wave function. While the $[ud]_{0^+}$ isoscalar-scalar diquark (SC) is dominant, material contributions also owe to the $\{uu\}_{1^+}$, $\{ud\}_{1^+}$ isovector-axialvector correlations (AV).

separation into spin and orbital angular momentum components carried by the system's identified constituents [14]. Hence, potential model wave functions might only provide a rudimentary guide to baryon structure; especially, as will become apparent, insofar as assignments to SU(6) ⊗ O(3) multiplets are concerned.

An alternative lies in calculations of the bound-state pole position and residue in the six-point Schwinger function that describes three-quark–to–three-quark scattering. This is the matrix element upon which simulations of lattice-QCD focus in order to extract baryon masses [15,16]. It is also the basis for studies of baryon composition using continuum Schwinger function methods (CSMs) [8,17,18]. In this framework, the problem is expressed via a Poincaré-covariant three-body Faddeev equation whose solution yields the masses and bound state amplitudes of all baryons in the channel under consideration. Baryon properties have been computed [19–22] at leading-order in a systematic, symmetry-preserving truncation scheme [23–25]; and efforts are underway to implement more sophisticated truncations [26].

Meanwhile, a simplification of the full three-body problem continues to be employed with success. Namely, the interacting quark + diquark picture, illustrated in Fig. 1, that was derived from the three-body equation in Refs. [27–30]. The approximation is efficacious because any interaction that is able to generate Nambu-Goldstone modes as dressed-quark+antiquark bound-states and reproduce the measured value of their leptonic decay constants, must also produce strong color-antitriplet correlations between any two dressed quarks contained within a hadron [31]. In general, for light-quark systems, the following diquark correlations are possible: isoscalar-scalar, $(I, J^P = 0, 0^+)$; isovector-axialvector; isoscalar-pseudoscalar; isoscalar-vector; and isovector-vector. Within a given system, channel dynamics determines the relative strengths of these correlations. Herein, owing to the fact that $I = \frac{3}{2}$ baryons cannot be built from $I = 0$ diquarks, we just need to consider $(1, 1^\pm)$ correlations.

It is worth stressing that the diquark correlations discussed herein are fully dynamical, appearing in a Faddeev kernel which requires their continual breakup and reformation. Hence, they are very different from the pointlike, static diquarks introduced more than fifty years ago [32] with a view to solving the so-called "missing resonance" problem [33]. This essentially active character of the valence quarks within diquarks entails that the spectrum produced by Fig. 1 possesses a richness that cannot be explained by two-body models, something also found in numerical simulations of lattice-regularized QCD [15].

An analysis of the four lowest-lying $(\frac{1}{2}, \frac{1}{2}^\pm)$ baryons—the nucleon and some kindred systems—made using the quark + diquark framework is presented elsewhere [34]. It was found therein that $(0, 0^+)$ and $(1, 1^+)$ diquarks dominate the wave functions of the lightest $(\frac{1}{2}, \frac{1}{2}^+)$ doublets. This is illustrated for the nucleon ground-state in Fig. 2: roughly 60% of the proton's canonical normalization constant is provided by the $(0, 0^+)$ correlation, but the remainder owes to the $(1, 1^+)$ correlation and constructive $(0, 0^+) \otimes (1, 1^+)$ interference. (The canonical normalization constant is related to the $Q^2 = 0$ value of the charge form factors associated with the electrically charged members of a given hadron multiplet: in this case, that is the proton Dirac form factor.) As explained elsewhere [35,36], the size of the $(1, 1^+)$-linked contributions is sufficient to explain the measured ratio of proton valence-quark distribution functions [37,38].

Furthermore, as shown for the nucleon in Fig. 3, projected into the rest frame, these wave functions have significant S-wave components; yet they also contain material P-wave structures and the canonical normalization receives measurable S ⊗ P-wave interference contributions. In addition [34], the first $\frac{1}{2}^+$ excited state may fairly be described as the radial excitation of the ground state.
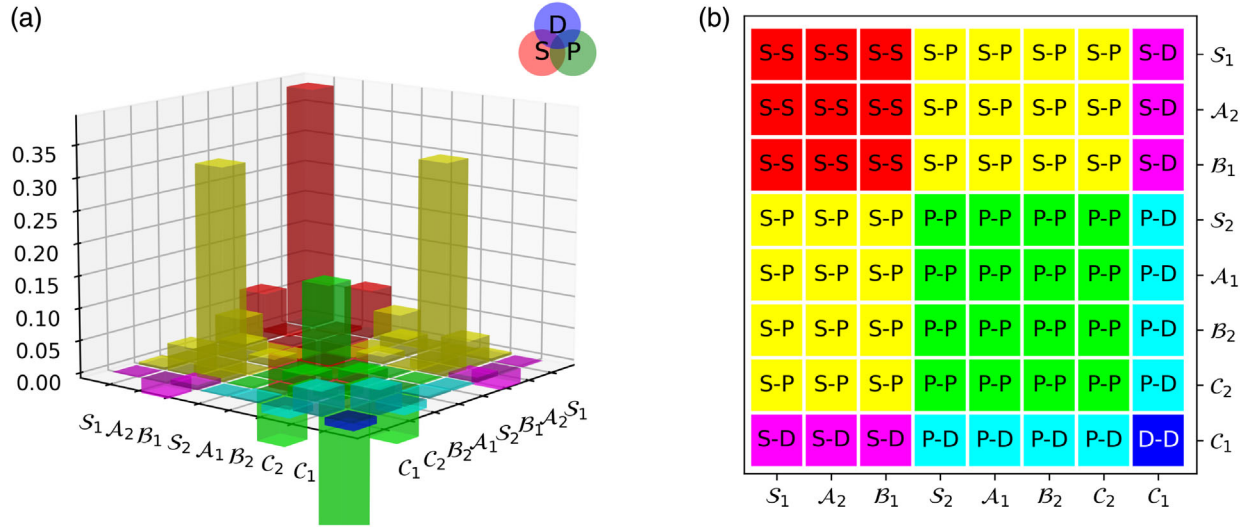
FIG. 3.   Panel (a). Contributions of the various quark + diquark orbital angular momentum components to the canonical normalization of the Poincaré-covariant nucleon wave function after rest-frame projection: there are both positive (above plane) and negative (below plane) contributions to the overall positive normalization. The values drawn are listed in Table IV. Panel (b). Legend for interpretation of Panel A, identifying interference between the distinct orbital angular momentum basis components. Decomposition details are provided in Table I. It follows the scheme described in Refs. [39,40] and uses a pictorial representation based on that in Ref. [41].

In these outcomes, there are some parallels with quark model expectations for these states.

On the other hand, the related $(\frac{1}{2}, \frac{1}{2}^-)$ doublets fit a different picture [34]: $(0, 1^-)$ diquarks play an important role; the wave functions are predominantly P-wave in nature, but contain significant S-wave components; and the heavier states are not simply radial excitations of their lighter partners.

Notably, in quantum field theory, all differences between positive- and negative-parity states can be attributed to chiral symmetry breaking, as highlighted by the ρ-a_1 meson complex [26,42–44]. In the light-quark sector, such symmetry breaking is almost entirely dynamical. Dynamical chiral symmetry breaking (DCSB) is a corollary of emergent hadron mass (EHM) [45–48]; hence, quite probably linked tightly with confinement, which requires a ~ 1 fm^{-1} mass-scale to be effective [49]. Consequently, experiments that can test predictions made for differences between parity partners in the hadron spectrum are valuable. These features imbue quantum field theory studies of $(\frac{3}{2}, \frac{3}{2}^\pm)$ baryons with particular interest.

Our approach to the $(\frac{3}{2}, \frac{3}{2}^\pm)$-baryon bound-state problems is sketched in Sec. II. Solutions for the masses and Poincaré-covariant wave functions of the lowest-lying such states are described and dissected in Sec. III. Section IV provides a summary and perspective.

II. BOUND STATE EQUATIONS

In studying $(\frac{3}{2}, \frac{3}{2}^\pm)$ baryons, we follow the analysis of $(\frac{1}{2}, \frac{1}{2}^\pm)$ states in Ref. [34]. For instance: we assume isospin symmetry throughout; the diquark correlation amplitudes,

Γ^{J^P}, are similar; the light-quark and diquark propagators, S, D^{J^P}, are unchanged—see Appendix A 1; and the effective masses of the relevant diquark correlations are (in GeV)

$$m_{\{uu\}_{1^+}} = 0.9, \qquad m_{\{uu\}_{1^-}} = 1.4. \qquad (1)$$

The mass splitting here is commensurate with that in the ρ-a_1 complex [7]. On the other hand, since the negative-parity diquarks are heavy, we emulate Ref. [50] Sec. 4.1.4 in electing not to include the g_{DB} channel-coupling suppression-factor discussed in Ref. [34] Sec. II.E.

Focusing on the electric charge $e_\Delta = +2$ state without loss of generality, the Faddeev equation for a $(\frac{3}{2}, \frac{3}{2}^{P=\pm})$ baryon can be written [[51] Sec. 2.1, [52] Sec. 4.1]:

$$\sum_{p=\pm} \psi_\lambda^{pP}(k; Q) = 8 \sum_{p=\pm} \int \frac{d^4\ell}{(2\pi)^4} \mathcal{M}_{\lambda\mu}^p(k, \ell; Q) \psi_\mu^{pP}(\ell; Q).$$

$$(2)$$

Here, $Q^2 = \hat{Q}^2 M^2 = -M^2$, M is the baryon's mass,

$$\psi_\lambda^P(k; Q) = \sum_{p=\pm} \psi_\lambda^{pP}(k; Q), \qquad (3a)$$

$$\psi_\lambda^{pP}(k; Q) = \mathcal{T}_{\lambda\rho}^{pP}(k; Q) u_\rho(Q; r), \qquad (3b)$$

$$\mathcal{T}_{\lambda\rho}^{+P}(k; Q) = \sum_{i=1}^{8} v_+^i(k^2, k \cdot Q) \mathcal{G}^P \mathcal{V}_{\lambda\rho}^i(k; Q), \qquad (3c)$$

$$\mathcal{T}_{\lambda\rho}^{-P}(k; Q) = \sum_{i=1}^{8} v_-^i(k^2, k \cdot Q) \mathcal{G}^\mp \mathcal{V}_{\lambda\rho}^i(k; Q), \qquad (3d)$$

where: for a given baryon, $p = +$ indicates the axial-vector component of its amplitude and $p = -$, the vector component; $\mathcal{G}^{P=+(-)} = \mathbb{I}_{\mathrm{D}}(i\gamma_5)$; and, with $T_{\mu\nu} = \delta_{\mu\nu} + \hat{Q}_\mu\hat{Q}_\nu$, $\gamma_\mu^\perp = T_{\mu\nu}\gamma_\nu$, $k_\mu^\perp = T_{\mu\nu}k_\nu$, $\hat{k}_\mu^\perp\hat{k}_\mu^\perp = 1$,

$$\mathcal{V}^1_{\lambda\rho}(k;Q) = \delta_{\lambda\rho}\mathbb{I}_{\mathrm{D}}, \tag{4a}$$

$$\mathcal{V}^2_{\lambda\rho}(k;Q) = \frac{i}{\sqrt{5}}[2\gamma_\lambda^\perp\hat{k}_\rho^\perp - 3\delta_{\lambda\rho}\gamma\cdot\hat{k}^\perp], \tag{4b}$$

$$\mathcal{V}^3_{\lambda\rho}(k;Q) = -i\gamma_\lambda^\perp\hat{k}_\rho^\perp, \tag{4c}$$

$$\mathcal{V}^4_{\lambda\rho}(k;Q) = \sqrt{3}\hat{Q}_\lambda\hat{k}_\rho^\perp, \tag{4d}$$

$$\mathcal{V}^5_{\lambda\rho}(k;Q) = 3\hat{k}_\lambda^\perp\hat{k}_\rho^\perp - \delta_{\lambda\rho} - \gamma_\lambda^\perp\hat{k}_\rho^\perp\gamma\cdot\hat{k}^\perp, \tag{4e}$$

$$\mathcal{V}^6_{\lambda\rho}(k;Q) = \gamma_\lambda^\perp\hat{k}_\rho^\perp\gamma\cdot\hat{k}^\perp, \tag{4f}$$

$$\mathcal{V}^7_{\lambda\rho}(k;Q) = -i\sqrt{3}\hat{Q}_\lambda\hat{k}_\rho^\perp\gamma\cdot\hat{k}^\perp, \tag{4g}$$

$$\mathcal{V}^8_{\lambda\rho}(k;Q) = \frac{i}{\sqrt{5}}[\delta_{\lambda\rho}\gamma\cdot\hat{k}^\perp + \gamma_\lambda^\perp\hat{k}_\rho^\perp - 5\hat{k}_\lambda^\perp\hat{k}_\rho^\perp\gamma\cdot\hat{k}^\perp] \tag{4h}$$

are a complete set of Dirac-matrix-valued basis vectors, sufficient to deliver $J = \frac{3}{2}$ amplitudes and wave functions that are Poincaré-covariant.

In Eq. (11b), $u_\rho(Q;r)$ is a Rarita-Schwinger spinor:

$$\frac{1}{2M}\sum_{r=-3/2}^{3/2} u_\mu(Q;r)\bar{u}_\nu(Q;r) = \Lambda_+(Q)R_{\mu\nu}, \tag{5}$$

$\Lambda_+(Q) = (-i\gamma\cdot Q + M)/(2M)$,

$$R_{\mu\nu} = \delta_{\mu\nu}\mathbb{I}_{\mathrm{D}} - \frac{1}{3}\gamma_\mu\gamma_\nu + \frac{2}{3}\hat{Q}_\mu\hat{Q}_\nu\mathbb{I}_{\mathrm{D}} - \frac{i}{3}[\hat{Q}_\mu\gamma_\nu - \hat{Q}_\nu\gamma_\mu]. \tag{6}$$

(Details of our Euclidean metric conventions are presented elsewhere [[53] Appendix B]).

The kernel in Eq. (2) can now be constructed from Fig. 1, e.g., following the pattern in Ref. [[52] Sec. 4.1]:

$$\mathcal{M}^\pm_{\lambda\mu} = \Gamma^{1^\pm}_\sigma(k_q - \ell_{qq}/2; \ell_{qq})S^T(\ell_{qq} - k_q)$$
$$\times \bar{\Gamma}^{1^\pm}_\lambda(\ell_q - k_{qq}/2; -k_{qq})S(\ell_q)D^{1^\pm}_{\sigma\mu}(\ell_{qq}), \tag{7}$$

where $\ell_q = \ell + Q/3$, $k_q = k + Q/3$, $\ell_{qq} = -\ell + 2Q/3$, $k_{qq} = -k + 2Q/3$, and "T" denotes matrix transpose.

The $(1, 1^\pm)$ correlation amplitudes are explained in Ref. [[34], Eq. (1)], but it is useful to recapitulate:

$$\Gamma^{1^+}_\mu(k;K) = ig_{1^+}\gamma_\mu C\mathcal{F}(k^2/\omega^2_{1^+}), \tag{8a}$$

$$\Gamma^{1^-}_\mu(k;K) = ig_{1^-}[\gamma_\mu, \gamma\cdot\hat{K}]\gamma_5 C\mathcal{F}(k^2/\omega^2_{1^-}), \tag{8b}$$

where $C = \gamma_2\gamma_4$ is the charge conjugation matrix, $\mathcal{F}(z)$ is given in Eq. (A5), and the correlation widths are defined by the related masses [[34] Eq. (5)]: $\omega^2_{1^\pm} = m^2_{1^\pm}/2$. (The color and flavor structure has already been absorbed into Eq. (7).) The amplitudes are canonically normalized [[34] Eq. (3)], which entails:

$$g_{1^+} = 12.7, \qquad g_{1^-} = 1.58. \tag{9}$$

Since it is the coupling-squared which appears in the Faddeev kernel, $(1, 1^+)$ diquarks should be the overwhelmingly favored correlations in all states considered herein. This fact lends support to baryon spectrum calculations made using a symmetry-preserving regularization of a vector × vector contact interaction, which cannot support $(1, 1^-)$ diquarks [50,54].

Using the information above, the masses and Faddeev amplitudes of the ground- and first-excited state in both the positive- and negative-parity channels can be obtained straightforwardly by solving the Faddeev equation— Fig. 1, Eq. (2)—using readily available software [55,56].

Importantly for what follows in connection with angular momentum decompositions of baryon properties, the unamputated Faddeev wave function is recovered from the amplitude by reattaching the quark and diquark propagator legs:

$$\Psi^\pm_{\bar{\lambda}}(k;Q) = \sum_{p=\pm}\Psi^{p\pm}_{\bar{\lambda}}(k;Q) \tag{10a}$$

$$= \sum_{p=\pm}S(k_q)D^{1p}_{\lambda\mu}(k_d)\psi^{p\pm}_\mu(k;Q). \tag{10b}$$

It is only when working with the wave function that meaningful angular momentum decompositions become available. It is straightforward to reformulate the Faddeev equation such that the wave function is returned as the solution eigenvector instead of the amplitude.

Decomposing $\Psi^\pm_{\bar{\lambda}}(k;Q)$ over the basis matrix-vectors in Eq. (4), following the pattern in Eq. (3) but with distinct coefficient functions, written herein as $\{w^i_\pm | i = 1, \ldots, 8\}$, viz.

$$\Psi^\pm_{\bar{\lambda}}(k;Q) = \sum_{p=\pm}\Psi^{p\pm}_{\bar{\lambda}}(k;Q), \tag{11a}$$

$$\Psi^{p\pm}_{\bar{\lambda}}(k;Q) = \mathcal{F}^{p\pm}_{\lambda\rho}(k;Q)u_\rho(Q;r), \tag{11b}$$

$$\mathcal{T}^{+\pm}_{\lambda\rho}(k;Q) = \sum_{i=1}^{8}w^i_+(k^2, k\cdot Q)\mathcal{G}^\pm\mathcal{V}^i_{\lambda\rho}(k;Q), \tag{11c}$$

$$\mathcal{T}^{-\pm}_{\lambda\rho}(k;Q) = \sum_{i=1}^{8}w^i_-(k^2, k\cdot Q)\mathcal{G}^\mp\mathcal{V}^i_{\lambda\rho}(k;Q), \tag{11d}$$

TABLE I. Working with the wave function defined in Eq. (10), decomposed over the basis matrix-vectors in Eq. (4), with coefficient functions $\{w_{\pm}^i | i = 1, \ldots, 8\}$, and projected into the rest frame, one has the tabulated $J = \frac{3}{2} = L + S$ angular momentum decomposition. The last row lists the associated spectroscopic label, with the $J = \frac{3}{2}$ subscript suppressed.

L	0	1	1	2	2	3
S	$\frac{3}{2}$	$\frac{3}{2}$	$\frac{1}{2}$	$\frac{3}{2}$	$\frac{1}{2}$	$\frac{3}{2}$
$\Psi^{p=\pm}$	$w_{\pm}^1$	$w_{\pm}^2$	$w_{\pm}^{3,4}$	$w_{\pm}^5$	$w_{\pm}^{6,7}$	$w_{\pm}^8$
	^4S	^4P	^2P	^4D	^2D	^4F

then one has the angular momentum associations listed in Table I.

III. SOLUTIONS AND THEIR FEATURES

A. Quark core

Solving for the complete Faddeev amplitude, one obtains the masses listed in Table II. Notably, the kernel in Fig. 1 omits all those contributions which may be linked with meson-baryon final-state interactions, *viz.* the terms resummed in dynamical coupled channels (DCC) models in order to transform a bare-baryon into the observed state [57–60]. Our Faddeev amplitudes should thus be viewed as describing the *dressed-quark core* of the bound-state, not the completely-dressed, observable object [52,61,62]; hence, the masses are uniformly too large. For comparison with experiment, we subtract the mean value of the difference between our calculated masses and the real part of the related empirical pole-positions: $\delta_{\rm MB} = 0.17$ GeV. This value matches the offset between bare and dressed $\Delta(1232)\frac{3}{2}^+$ masses determined in the DCC analysis of Ref. [58]. The resulting comparison is displayed in Fig. 4: the calculated level orderings and splittings match well with experiment. The simplicity of the Δ-baryon Faddeev

TABLE II. Calculated masses of lowest-lying $(\frac{3}{2}, \frac{3}{2}^{\pm})$ Δ-baryons: the indicated uncertainty stems from a $\pm 5\%$ change in the $(1, 1^{\pm})$ diquark masses in Eq. (1). The mean difference between central predicted masses and the real-part of the empirical pole positions is $\delta_{\rm MB} = 0.17$ GeV. The remaining columns display the mass fractions contributed by the $(1, 1^{\pm})$ diquarks, described in connection with Eq. (12), and analogous amplitude fractions, with the latter defined via Eqs. (15).

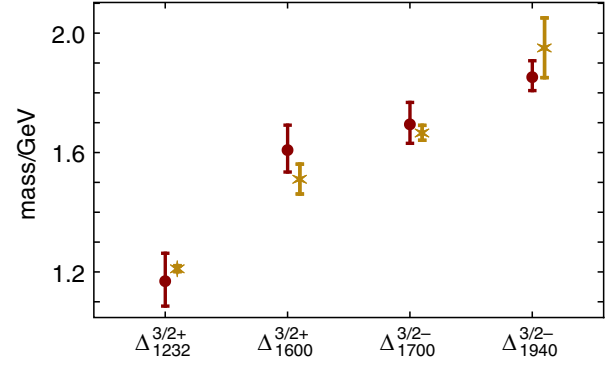|	Mass/GeV		Mass %		Amplitude %	
	1^+	1^+ & 1^-	1^+	1^-	1^+	1^-
$\Delta(1232)\frac{3}{2}^+$	1.346	1.346(89)	99.98	0.02	96.97	3.03
$\Delta(1600)\frac{3}{2}^+$	1.786	1.786(79)	99.96	0.04	96.57	3.43
$\Delta(1700)\frac{3}{2}^-$	1.872	1.871(69)	99.98	0.02	94.20	5.80
$\Delta(1940)\frac{3}{2}^-$	2.030	2.043(50)	99.37	0.63	88.73	11.27

FIG. 4. Real part of empirical pole position for each identified baryon [7] (gold asterisk) compared with calculated masses in Table II after subtracting $\delta_{\rm MB} = 0.17$ GeV from each of the latter (red circles). The calculated values are drawn with an uncertainty stemming from a $\pm 5\%$ change in the $(1, 1^{\pm})$ diquark masses.

equations, which are effectively single-diquark-channel problems owing to Eq. (9), is instrumental in delivering this outcome so straightforwardly. $J = \frac{1}{2}$ systems are more complicated because they potentially involve interference between contributions from five distinct diquark correlations [34], the character of which must be properly expressed in the Faddeev kernel.

The diquark mass fractions in Table II are obtained as follows. (i) Solve for the baryon mass without $(1, 1^-)$ diquarks to obtain $m_{\Delta}^{1^+}$. (ii) Solve with both diquarks included to obtain $m_{\Delta}^{1^{\pm}}$. (iii) The listed fractions are

$$\text{mass}^{1^+} = m_{\Delta}^{1^+} / m_{\Delta}^{1^{\pm}}, \qquad \text{mass}^{1^-} = 1 - \text{mass}^{1^+}. \quad (12)$$

Considering the Poincaré-covariant Faddeev wave functions obtained for each state, it is worth recording some remarks about the zeroth Chebyshev projection of each term in Eq. (11):

$$w^j(k^2) = \frac{2}{\pi} \int_{-1}^1 dx \sqrt{1 - x^2}\, w^j(k^2, x\sqrt{k^2 Q^2}). \quad (13)$$

The positive-parity states are straightforward: $\Delta(1232)\frac{3}{2}^+$—no such function with significant magnitude possesses a zero, an outcome consistent with the picture of this system as a radial ground state; and $\Delta(1600)\frac{3}{2}^+$—every function with significant magnitude displays a single zero; hence, as explained in connection with meson radial excitations [63,64], this state has the appearance of the radial excitation of the $\Delta(1232)\frac{3}{2}^{\pm}$. These features are illustrated in Figs. 5(a) and 5(b).

On the other hand, as found with $(\frac{1}{2}, \frac{1}{2}^-)$ states [34], the wave functions of the negative-parity Δ-baryons are much more complex. This is illustrated in Figs. 5(c) and 5(d), which show that for both $\Delta(1700)\frac{3}{2}^-$ and $\Delta(1940)\frac{3}{2}^-$ most
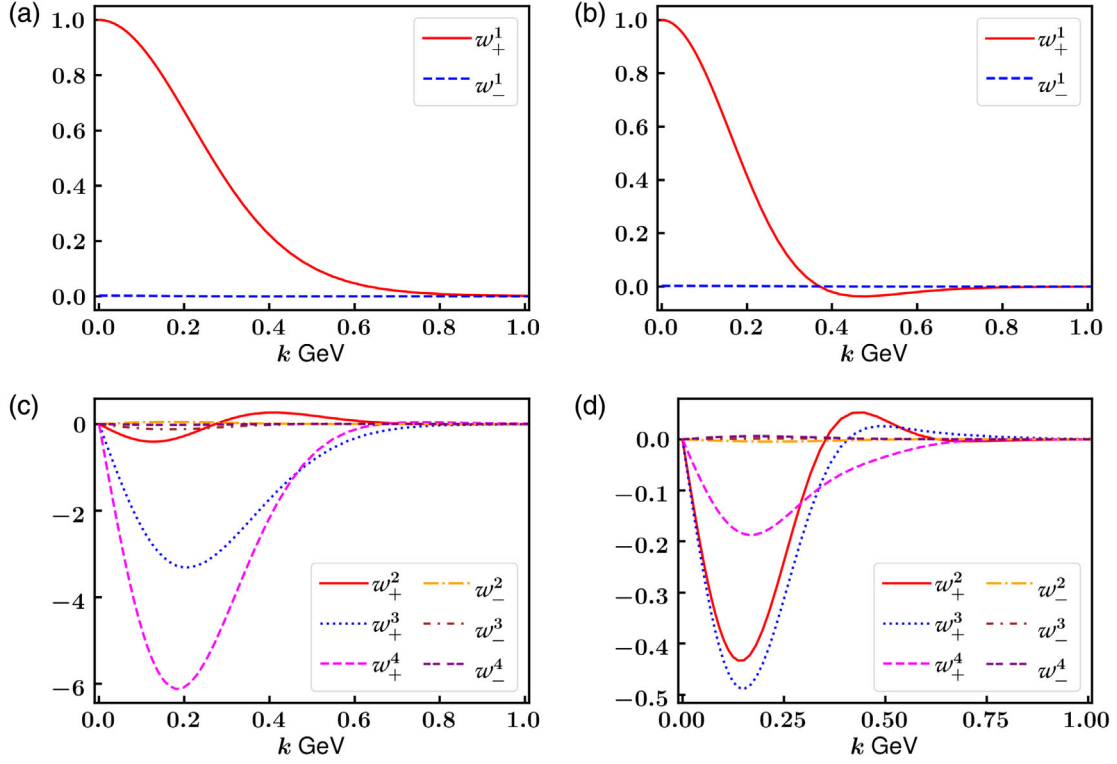
FIG. 5. Zeroth Chebyshev moments—Eq. (13). Upper panels. rest-frame S-wave components in wave functions of positive parity baryons: (a) $\Delta(1232)\frac{3}{2}^+$; (b) $\Delta(1600)\frac{3}{2}^+$. These components are dominant in both states, as evident in Figs. 6, 8(a), and 8(b). Lower panels. Rest-frame P-wave components in wave functions of negative parity baryons: (c) $\Delta(1700)\frac{3}{2}^-$; (d) $\Delta(1940)\frac{3}{2}^-$. As highlighted by Figs. 6, 8(c), and 8(d), these components are dominant in the $\Delta(1700)\frac{3}{2}^-$, but subdominant in the $\Delta(1940)\frac{3}{2}^-$.

of the wave function projections, Eq. (13), possess a zero; and this is true for more of the $\Delta(1940)\frac{3}{2}^-$ projections.

It is worth noting that when a zero exists, it lies within the domain $\frac{1}{3}$ fm $\lesssim \frac{1}{k} \lesssim \frac{1}{2}$ fm, i.e., at length-scales smaller than the bound-state radii. This is similarly so of $(\frac{1}{2}, \frac{1}{2}^\pm)$ bound-states [[34] Figs. 4 and 5] and also vector mesons [[65] Fig. 5]. The zero in the leading Chebyshev amplitude of the pion's first radial excitation is found even deeper: $\frac{1}{k} \approx \frac{1}{5}$ fm [[65] Fig. 4].

Such structural predictions for the properties of $(\frac{3}{2}, \frac{3}{2}^\pm)$ baryons can be tested via comparisons with data obtained on the Q^2-dependence of nucleon-to-resonance transition form factors [11–13].

B. Diquark fractions

It is apparent from Table II that, so far as the masses are concerned, neglecting $(1, 1^-)$ diquark correlations is an excellent approximation. One can also consider their relative contribution to the Faddeev amplitude, which may be defined following Ref. [34]. Namely, with

$$n^j = \int \frac{d^4k}{(2\pi)^4} |u^j(k^2, k \cdot Q)|^2, \qquad (14)$$

where $u^j \in \{v_+^{i,\dots,8}\} \cup \{v_-^{i,\dots,8}\}$, then, for each Δ-baryon, one computes

$$\mathbb{N}_{p=\pm} = \sum_{j\in\{v_p^{i,\dots,8}\}} n^j, \qquad \mathbb{D} = \mathbb{N}_+ + \mathbb{N}_- \qquad (15)$$

and compares the results for $\mathbb{F}_\pm = \mathbb{N}_\pm/\mathbb{D}$, which are listed, respectively, in the final two columns of Table II. Unsurprisingly, the negative-parity diquarks feature most prominently in the negative-parity baryons; but even in these states, they are very much subdominant.

C. Angular momentum decompositions

We judge it to be of particular interest to expose the rest-frame angular momentum structure of the $(\frac{3}{2}, \frac{3}{2}^\pm)$ systems produced by our Poincaré covariant framework. As a first step toward that goal, we solved the Faddeev equation for the wave function of each baryon in its rest frame by changing and steadily increasing the orbital angular momentum complexity: (i) S-wave only; (ii) P-wave only; (iii) D-wave only; (iv) S + P-wave only; etc. The results are presented in Table III.

Table III rewards careful inspection. For instance, it reveals that in every channel a solution is obtained using only one partial wave—S, P, D, or F, or any subset of the

TABLE III. Calculated masses of the lowest-lying $(\frac{3}{2}, \frac{3\pm}{2})$ Δ-baryons (in GeV) as obtained by stepwise including different orbital angular momentum components in the rest-frame Faddeev wave function. The italicized entries highlight the lowest mass obtained in solving with a single partial wave.

Δ	S	P	D	F	SP	SD	PD	SPD	SPDF
$(1232)\frac{3+}{2}$	*1.35*	2.03	1.80	2.35	1.35	1.36	1.83	1.35	1.35
$(1600)\frac{3+}{2}$	*1.80*	2.22	2.10	2.48	1.84	1.76	2.02	1.78	1.79
$(1700)\frac{3-}{2}$	1.90	*1.80*	2.18	2.17	1.89	1.90	1.80	1.87	1.87
$(1940)\frac{3-}{2}$	*2.06*	2.20	2.27	2.38	2.05	2.05	2.19	2.05	2.04

complete array of partial waves. Plainly, notwithstanding its apparent simplicity, the Faddeev kernel in Eq. (7) is very effective at binding $(\frac{3}{2}, \frac{3\pm}{2})$ baryons. Furthermore, considering only a single partial wave, then the lightest mass obtained should serve as a reliable indicator of the dominant orbital angular momentum component in the state. Using this definition, one arrives at the following assignments: $\Delta(1232)\frac{3+}{2}$ and $\Delta(1600)\frac{3+}{2}$ are largely S-wave in nature, but with contributing P-, D-wave components; $\Delta(1700)\frac{3-}{2}$ is primarily a P-wave state, but possesses measurable S-, D-wave components; and, surprisingly, because it runs counter to quark model notions [[7] Sec. 15], $\Delta(1940)\frac{3-}{2}$ is predominantly a S-wave state, with small contributions from other partial waves. These observations are illustrated in Fig. 6.

Hadron masses are simple observables in the sense that they are infrared dominated quantities, whose values are not especially sensitive to structural details expressed in hadron wave functions. Consequently, the simplicity evident in Fig. 6 is somewhat misleading, as highlighted again
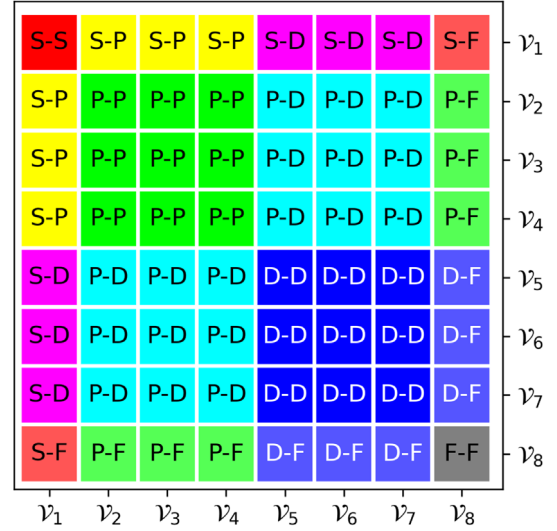
FIG. 7. Legend for interpretation of Figs. 8(a)–8(d), identifying interference between the various identified orbital angular momentum basis components in the baryon rest frame.

when one isolates the distinct contributions from each partial wave to the associated canonical normalization. Using the assignments specified in Fig. 7, those decompositions are depicted in Fig. 8, being drawn from the numerical values collected in Appendix A 2. Since $(1, 1^-)$ diquarks make negligible contributions, only the $(1, 1^+)$ contributions are reported and drawn.

Considering Fig. 8(a), one sees that, evaluated in the rest frame, the canonical normalization of the $\Delta(1232)\frac{3+}{2}$ is largely determined by S-wave components, but there are significant, constructive P wave contributions and also strong $S \otimes P$-wave destructive interference terms. This structural picture of the $\Delta(1232)\frac{3+}{2}$ has been confirmed by comparisons with data on the $\gamma + p \rightarrow \Delta(1232)$ transition form factors [53,66,67].

Moving to Fig. 8(b), although S-wave contributions are dominant in the $\Delta(1600)\frac{3+}{2}$, there are prominent D-wave components, material $P \otimes D$-wave interference contributions, and numerous F-wave induced interference terms. Enhanced higher partial waves are also seen in related three-body Faddeev equation studies of the $\Delta(1600)\frac{3+}{2}$ [68,69]. This quark + diquark structural picture of the $\Delta(1600)\frac{3+}{2}$ has been used to calculate $\gamma + p \rightarrow \Delta(1600)$ transition form factors [67]. Those predictions are currently being tested through analysis of $\pi^+\pi^- p$ electroproduction data collected at Jefferson Lab [70], with preliminary results confirming the quark + diquark picture [71].

The $\Delta(1700)\frac{3-}{2}$ normalization strengths are displayed in Fig. 8(c). Confirming expectations raised by Table III, P-wave components are dominant, but D-wave and $P \otimes D$ interference is evident, and also some $D \otimes F$ contributions. $\Delta(1700)\frac{3-}{2}$ electrocoupling data are available from Jefferson Lab [72–74]. However, they only reach $Q^2 \approx 1.5m_p^2$; hence,
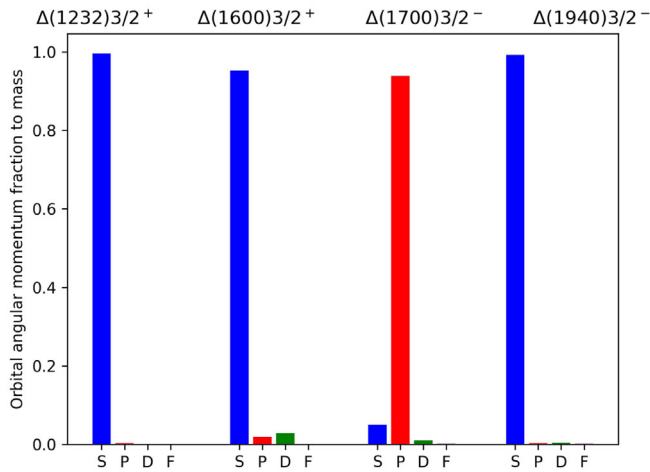

FIG. 6. Pictorial representation of Table III. Mass fraction contribution from each rest frame partial wave in the baryon wave function, computed as follows: $\Delta(1232)\frac{3+}{2}$, $\Delta(1600)\frac{3+}{2}$, $\Delta(1940)\frac{3-}{2}$—begin with S-wave, then add P, D, F; and $\Delta(1700)\frac{3-}{2}$—begin with P-wave, then add S, D, F.
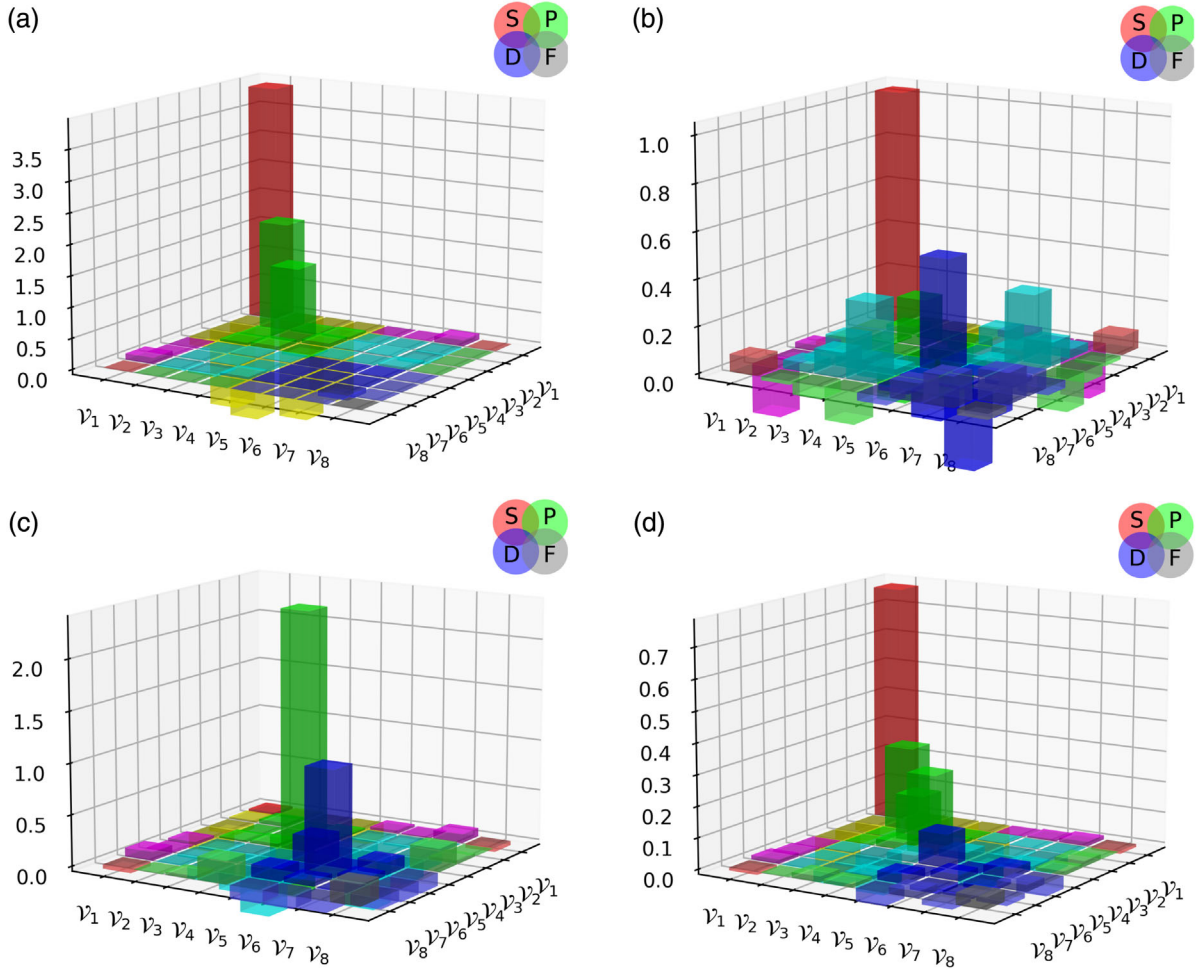
FIG. 8. Rest frame quark + $(1, 1^+)$-diquark orbital angular momentum content of $(\frac{3}{2}, \frac{3}{2}^{\pm})$ states considered herein, as measured by the contribution of the various components to the associated canonical normalization constant: (a) $\Delta(1232)\frac{3}{2}^+$; (b) $\Delta(1600)\frac{3}{2}^+$; (c) $\Delta(1700)\frac{3}{2}^-$; and (d) $\Delta(1940)\frac{3}{2}^-$—drawn with reference to Table I and the basis in Eq. (4). There are both positive (above plane) and negative (below plane) contributions to the overall normalizations, which are all positive.

are insufficient to test our $\Delta(1700)\frac{3}{2}^-$ structure predictions. It would nevertheless be worthwhile to use our wave functions as the basis for calculating the $\gamma + p \rightarrow \Delta(1700)$ transition form factors, providing motivation and support for extraction of $\Delta(1700)\frac{3}{2}^-$ electrocouplings on $2 < Q^2/\text{GeV}^2 < 5$ from existing $\pi^+\pi^- p$ electroproduction data [75,76].

The $\Delta(1940)\frac{3}{2}^-$ normalization strengths are displayed in Fig. 8(d). Unlike the other systems studied herein, this is only a "∗∗" state [7]; and no electrocoupling data are available, although they are expected to be collected in future Jefferson Lab $\pi^+\pi^- p$ electroproduction experiments [70]. Such data would be valuable because our analysis shows that the $\Delta(1940)\frac{3}{2}^-$ is potentially a peculiar system, *viz.* a negative-parity baryon whose rest-frame wave function is largely S-wave in character. Even if this outcome were to indicate a failure of our Faddeev equation in describing some higher baryon resonances, resolving the question is necessary in order to ensure arrival at a reliable

Poincaré covariant description of baryon spectra and structure.

IV. SUMMARY AND PERSPECTIVE

A Poincaré-covariant Faddeev equation [Fig. 1], whose kernel is built using dressed-quark and nonpointlike diquark degrees-of-freedom, with binding generated by the exchange of a dressed-quark, which emerges as one diquark breaks-up and is absorbed into formation of another, was used to calculate the mass and Faddeev wave functions of the lowest-lying $(I, J^P = \frac{3}{2}, \frac{3}{2}^{\pm})$ baryons. This approach has previously been used widely to deliver explanations of many baryon properties [31], with recent applications to parton distribution functions [35,36], the large-Q^2 behavior of elastic and transition form factors [77,78], and axial form factors [79,80]. It should, therefore, provide a sound approach to the study of Δ-baryons.

In principle, viewed from the quark + diquark perspective, $(\frac{3}{2}, \frac{3}{2}^{\pm})$ baryons can contain both $(1, 1^{+})$ and $(1, 1^{-})$ quark + quark correlations. However, our analysis revealed that $(1, 1^{-})$ diquarks may safely be neglected [Sec. III B]. In this case, the Poincaré-covariant wave functions of $(\frac{3}{2}, \frac{3}{2}^{\pm})$ systems contain eight independent terms, each characterized by a scalar function of two variables: k^{2}, $k \cdot Q$, where k is the quark + diquark relative momentum and Q is the bound-state total momentum. Projecting each of these functions to obtain their zeroth Chebyshev moment, one arrives at a collection of simpler functions, useful for developing insights. Reviewing their behavior [Sec. III A], we found that the $\Delta(1600)\frac{3}{2}^{+}$ exhibits characteristics which enable it to be interpreted as a radial excitation of the $\Delta(1232)\frac{3}{2}^{+}$. However, no such simple relationship was found to be viable for the $\Delta(1700)\frac{3}{2}^{-}$, $\Delta(1940)\frac{3}{2}^{-}$ states.

Although the $J = L + S$ separation of a baryon's total angular momentum into a sum of orbital angular momentum and spin is frame dependent, one may nevertheless make some contact with quark model pictures of $(\frac{3}{2}, \frac{3}{2}^{\pm})$ baryons by projecting their Poincaré-covariant Faddeev wave functions into the associated rest frames. Following this procedure [Sec. III C], we found that the angular momentum structure of all these Δ-baryons is far more complicated than generated by typical quark models. Nevertheless, drawing some link to quark models, the $\Delta(1232)\frac{3}{2}^{+}$ and $\Delta(1600)\frac{3}{2}^{+}$ baryons were found to be characterized by a dominant S-wave component, and the $\Delta(1700)\frac{3}{2}^{-}$ by a prominent P-wave. However, the $\Delta(1940)\frac{3}{2}^{-}$ did not fit this picture: contrary to quark model expectations, this state is S-wave dominated. Furthermore, combining the results from our analyses of their Poincaré-covariant quark + diquark Faddeev wave functions, we judged that negative parity Δ-baryons are not simply orbital angular momentum excitations of positive parity ground states. This conclusion matches that drawn elsewhere for $(\frac{1}{2}, \frac{1}{2}^{\pm})$ baryons [34]. Our structural predictions for the $\Delta(1940)\frac{3}{2}^{-}$ are likely to encourage new experimental efforts to extract reliable information about this poorly understood state from exclusive $\pi^{+}\pi^{-} p$ electroproduction data [75,76] and subsequent determination of this resonance's electroexcitation amplitudes.

It is here worth recalling that the interpolating fields for positive and negative parity hadrons can be related by chiral rotation of the quark spinors used in their construction. Hence, all differences between bound states in these channels are generated by chiral symmetry breaking, which is predominantly dynamical in the light-quark sector. Regarding the baryons discussed herein, this means that the following states are parity partners: $\Delta(1232)\frac{3}{2}^{+} - \Delta(1700)\frac{3}{2}^{-}$; and $\Delta(1600)\frac{3}{2}^{+} - \Delta(1940)\frac{3}{2}^{-}$.

The mass splitting between parity partners is usually ascribed to dynamical chiral symmetry breaking (DCSB); and we have seen herein that, again like the $(\frac{1}{2}, \frac{1}{2}^{\pm})$ sector, there are also marked differences between their internal structures. They, too, must owe to DCSB because the channels are identical when chiral symmetry is restored. DCSB is a corollary of emergent hadron mass, which may also be argued to underly confinement [46]; so, validating our predictions of marked structural differences between parity partners has the potential to reveal a great deal about key features of the Standard Model. A means to this end exists in resonance electroexcitation experiments on $Q^{2} \gtrsim 2m_{p}^{2}$.

There are many natural extensions of this study. For instance, solving Faddeev equations to reveal the composition of $(\frac{1}{2}, \frac{3}{2}^{\pm})$ and $(\frac{3}{2}, \frac{1}{2}^{\pm})$ baryons; calculation of the electromagnetic transition form factors mentioned above and those involving the additional states just indicated; analyses that focus on the structure of baryons containing heavier valence quarks; and the prediction of weak proton-to-Δ transition form factors, which may be crucial in understanding neutrino oscillation experiments [81]. Efforts are underway in each of these areas.

APPENDIX: SUPPLEMENTAL MATERIAL

1. Quark and diquark propagators

The dressed-quark propagator can be written:

$$S(k) = -i\gamma \cdot k\sigma_{V}(k^{2}) + \sigma_{S}(k^{2}) \tag{A1}$$

$$= 1/[i\gamma \cdot kA(k^{2}) + B(k^{2})]. \tag{A2}$$

In QCD, the wave function renormalization and dressed-quark mass:

$$Z(k^{2}) = 1/A(k^{2}), \qquad M(k^{2}) = B(k^{2})/A(k^{2}), \tag{A3}$$

TABLE IV. Proton—canonical normalization contributions broken into rest-frame quark + diquark orbital angular momentum components, defined with reference to the scheme described in Refs. [39,40]. Where there are numerical differences with Ref. [40], we consider the results here to be more reliable.

	$\mathcal{S}_1$	$\mathcal{A}_2$	$\mathcal{B}_1$	$\mathcal{S}_2$	$\mathcal{A}_1$	$\mathcal{B}_2$	$\mathcal{C}_2$	$\mathcal{C}_1$
$\mathcal{S}_1$	0.39	−0.01	0.08	0.05	0.00	0.00	0.00	0.00
$\mathcal{A}_2$	−0.01	0.00	−0.07	0.00	0.03	−0.02	0.04	−0.02
$\mathcal{B}_1$	0.08	−0.07	−0.04	0.00	0.01	0.00	0.33	0.01
$\mathcal{S}_2$	0.05	0.00	0.00	0.12	0.00	0.00	0.00	0.00
$\mathcal{A}_1$	0.00	0.03	0.01	0.00	0.00	0.02	−0.08	0.00
$\mathcal{B}_2$	0.00	−0.02	0.00	0.00	0.02	−0.01	0.02	−0.01
$\mathcal{C}_2$	0.00	0.04	0.33	0.00	−0.08	0.02	−0.24	0.04
$\mathcal{C}_1$	0.00	−0.02	0.01	0.00	0.00	−0.01	0.04	−0.01

respectively, receive strong momentum-dependent corrections at infrared momenta [46,82]: $Z(k^2)$ is suppressed and $M(k^2)$ enhanced. These features are an expression of DCSB.

Today, numerical solutions of the quark gap equation can readily be obtained, but the utility of an algebraic form for $S(k)$ when calculations require the evaluation of numerous multidimensional integrals is clear. An efficacious parametrization has been used extensively:

$$\bar{\sigma}_S(x) = 2\bar{m}\mathcal{F}(2(x+\bar{m}^2))$$
$$+ \mathcal{F}(b_1x)\mathcal{F}(b_3x)[b_0 + b_2\mathcal{F}(\epsilon x)], \quad \text{(A4a)}$$

$$\bar{\sigma}_V(x) = \frac{1}{x+\bar{m}^2}[1 - \mathcal{F}(2(x+\bar{m}^2))], \quad \text{(A4b)}$$

with $x = p^2/\lambda^2$, $\bar{m} = m/\lambda$,

$$\mathcal{F}(x) = \frac{1-e^{-x}}{x}, \quad \text{(A5)}$$

$\bar{\sigma}_S(x) = \lambda\sigma_S(k^2)$ and $\bar{\sigma}_V(x) = \lambda^2\sigma_V(k^2)$. The mass-scale, $\lambda = 0.566$ GeV, and parameter values

$\bar{m}$	b_0	b_1	b_2	b_3	
0.00897	0.131	2.90	0.603	0.185	(A6)

associated with Eqs. (A4) were fixed in a least-squares fit to light-meson observables [83,84]. ($\epsilon = 10^{-4}$ in Eq. (A4a) acts only to decouple the large- and intermediate-k^2 domains.)

The dimensionless light-quark current-mass in Eq. (A6) corresponds to $m = 5.08$ MeV and the parametrization yields the following Euclidean constituent-quark mass, defined as the solution of $k^2 = M^2(k^2)$: $M^E = 0.33$ GeV. The ratio $M^E/m = 65$ is one expression of DCSB in the parametrization of $S(k)$. It emphasises the marked enhancement of the dressed-quark mass function at infrared momenta.

TABLE V. $\Delta(1232)\frac{3}{2}^+$—canonical normalization contributions broken into rest-frame quark + $(1, 1^+)$-diquark orbital angular momentum components, defined with reference to Table I and the basis in Eq. (4).

	$\mathcal{V}_1$	$\mathcal{V}_2$	$\mathcal{V}_3$	$\mathcal{V}_4$	$\mathcal{V}_5$	$\mathcal{V}_6$	$\mathcal{V}_7$	$\mathcal{V}_8$
$\mathcal{V}_1$	3.90	−1.62	−1.28	−0.14	−0.01	0.00	0.10	0.00
$\mathcal{V}_2$	−1.69	1.77	0.02	0.04	−0.01	0.00	−0.03	0.00
$\mathcal{V}_3$	−1.27	0.03	1.21	0.06	0.02	0.01	−0.05	0.00
$\mathcal{V}_4$	−0.15	0.04	0.06	−0.06	0.01	0.00	0.04	0.00
$\mathcal{V}_5$	−0.01	−0.01	0.02	0.01	−0.01	0.00	0.01	0.00
$\mathcal{V}_6$	0.00	0.00	0.01	0.00	0.00	0.00	−0.01	0.00
$\mathcal{V}_7$	0.10	−0.03	−0.05	0.04	0.01	−0.01	−0.08	0.00
$\mathcal{V}_8$	0.00	0.00	0.00	0.00	0.00	0.00	0.00	0.00

The dressed-quark mass function generated by this parametrization compares well with that computed using sophisticated gap equation kernels [[34] Fig. A.1].

A propagator is associated with each quark + quark correlation in Fig. 1; and we use

$$D_{\mu\nu}^{1^\pm}(K) = \left[\delta_{\mu\nu} + \frac{K_\mu K_\nu}{m_{1^\pm}^2}\right]\frac{1}{m_{1^\pm}^2}\mathcal{F}(k^2/\omega_{1^\pm}^2). \quad \text{(A7)}$$

Our propagator representations ensure that the quarks and diquarks are confined within the baryons, as appropriate for colored objects: while the propagators are free-particlelike at spacelike momenta, they are pole-free on the timelike axis; and this is sufficient to ensure confinement via the violation of reflection positivity (see, e.g., Ref. [[49] Sec. 3]).

2. Quark + diquark angular momentum

Using our solutions of the Faddeev equations for the Poincaré-covariant baryon wave functions, evaluated in the rest frame, we computed the contributions of various quark + diquark orbital angular momentum components to each baryon's canonical normalization constant. The results are recorded in Table IV for the nucleon and Tables V–VIII for the Δ-baryons. It is from these tables that the images in Figs. 3 and 8 are drawn.

TABLE VI. $\Delta(1600)\frac{3}{2}^+$—canonical normalization contributions broken into rest-frame quark + $(1, 1^+)$-diquark orbital angular momentum components, defined with reference to Table I and the basis in Eq. (4).

	$\mathcal{V}_1$	$\mathcal{V}_2$	$\mathcal{V}_3$	$\mathcal{V}_4$	$\mathcal{V}_5$	$\mathcal{V}_6$	$\mathcal{V}_7$	$\mathcal{V}_8$
$\mathcal{V}_1$	1.03	0.00	−0.05	−0.02	0.03	−0.01	−0.21	0.07
$\mathcal{V}_2$	−0.01	0.03	−0.01	−0.04	0.08	0.03	0.04	−0.02
$\mathcal{V}_3$	−0.07	−0.01	0.20	−0.22	−0.08	0.04	0.11	−0.05
$\mathcal{V}_4$	−0.02	−0.04	−0.22	−0.15	−0.04	0.02	0.34	−0.14
$\mathcal{V}_5$	0.03	0.08	−0.09	−0.04	0.48	0.00	−0.02	−0.03
$\mathcal{V}_6$	−0.01	0.03	0.05	0.03	0.00	−0.02	−0.12	0.08
$\mathcal{V}_7$	−0.21	0.04	0.10	0.33	−0.02	−0.11	−0.30	0.13
$\mathcal{V}_8$	0.08	−0.02	−0.05	−0.14	−0.03	0.08	0.13	−0.02

TABLE VII. $\Delta(1700)\frac{3^-}{2}$—canonical normalization contributions broken into rest-frame quark $+ (1, 1^+)$-diquark orbital angular momentum components, defined with reference to Table I and the basis in Eq. (4).

	$\mathscr{V}_1$	$\mathscr{V}_2$	$\mathscr{V}_3$	$\mathscr{V}_4$	$\mathscr{V}_5$	$\mathscr{V}_6$	$\mathscr{V}_7$	$\mathscr{V}_8$
$\mathscr{V}_1$	0.03	0.02	−0.05	−0.16	0.03	0.01	0.08	−0.04
$\mathscr{V}_2$	0.02	0.04	0.00	0.02	−0.02	−0.03	0.00	0.00
$\mathscr{V}_3$	−0.05	0.00	−0.59	0.03	−0.10	0.00	−0.11	0.03
$\mathscr{V}_4$	−0.16	0.02	0.03	2.36	−0.25	−0.48	−0.17	0.22
$\mathscr{V}_5$	0.03	−0.02	−0.09	−0.25	0.26	0.01	0.12	−0.13
$\mathscr{V}_6$	0.01	−0.03	0.00	−0.48	0.01	1.04	0.05	−0.13
$\mathscr{V}_7$	0.08	0.00	−0.12	−0.17	0.12	0.05	−0.01	−0.11
$\mathscr{V}_8$	−0.04	0.00	0.03	0.22	−0.13	−0.13	−0.11	0.20

TABLE VIII. $\Delta(1940)\frac{3^-}{2}$—canonical normalization contributions broken into rest-frame quark $+ (1, 1^+)$-diquark orbital angular momentum components, defined with reference to Table I and the basis in Eq. (4).

	$\mathscr{V}_1$	$\mathscr{V}_2$	$\mathscr{V}_3$	$\mathscr{V}_4$	$\mathscr{V}_5$	$\mathscr{V}_6$	$\mathscr{V}_7$	$\mathscr{V}_8$
$\mathscr{V}_1$	0.77	−0.03	−0.03	−0.12	0.00	0.01	0.01	−0.01
$\mathscr{V}_2$	−0.03	0.27	0.00	0.00	0.00	0.00	0.00	0.00
$\mathscr{V}_3$	−0.03	0.00	0.15	0.02	−0.12	−0.01	−0.04	0.02
$\mathscr{V}_4$	−0.12	0.00	0.01	0.26	0.02	−0.02	0.01	0.01
$\mathscr{V}_5$	0.00	0.00	−0.12	0.02	0.11	0.00	0.03	−0.04
$\mathscr{V}_6$	0.01	0.00	−0.01	−0.02	0.00	0.02	−0.01	0.02
$\mathscr{V}_7$	0.01	0.00	−0.04	0.01	0.03	−0.02	−0.01	−0.02
$\mathscr{V}_8$	−0.01	0.00	0.02	0.01	−0.04	0.02	−0.02	0.04

[1] M. Gell-Mann, Quarks, Acta Phys. Austriaca Suppl. **9,** 733 (1972).

[2] S. Capstick and W. Roberts, Quark models of baryon masses and decays, Prog. Part. Nucl. Phys. **45,** S241 (2000).

[3] V. Crede and W. Roberts, Progress towards understanding baryon resonances, Rep. Prog. Phys. **76,** 076301 (2013).

[4] M. M. Giannini and E. Santopinto, The hypercentral constituent quark model and its application to baryon properties, Chin. J. Phys. **53,** 020301 (2015).

[5] W. Plessas, The constituent-quark model—Nowadays, Int. J. Mod. Phys. A **30,** 1530013 (2015).

[6] G. Eichmann, Theory introduction to baryon spectroscopy, arXiv:2202.13378.

[7] P. Zyla *et al.*, Review of particle physics, Prog. Theor. Exp. Phys. **2020,** 083C01 (2020).

[8] V. D. Burkert and C. D. Roberts, Colloquium: Roper resonance: Toward a solution to the fifty-year puzzle, Rev. Mod. Phys. **91,** 011003 (2019).

[9] S. J. Brodsky, A. Deur, and C. D. Roberts, Artificial dynamical effects in quantum field theory, Nat. Rev. Phys. (2022).

[10] R. J. Holt and C. D. Roberts, Distribution functions of the nucleon and pion in the valence region, Rev. Mod. Phys. **82,** 2991 (2010).

[11] D. Carman, K. Joo, and V. Mokeev, Strong QCD insights from excited nucleon structure studies with CLAS and CLAS12, Few Body Syst. **61,** 29 (2020).

[12] S. J. Brodsky *et al.*, Strong QCD from hadron structure experiments, Int. J. Mod. Phys. E **29,** 2030006 (2020).

[13] V. I. Mokeev and D. S. Carman, Photo- and electrocouplings of nucleon resonances, arXiv:2202.04180.

[14] F. Coester, Null plane dynamics of particles and fields, Prog. Part. Nucl. Phys. **29,** 1 (1992).

[15] R. G. Edwards, J. J. Dudek, D. G. Richards, and S. J. Wallace, Excited state baryon spectroscopy from lattice QCD, Phys. Rev. D **84,** 074508 (2011).

[16] Z. Fodor and C. Hoelbling, Light hadron masses from lattice QCD, Rev. Mod. Phys. **84,** 449 (2012).

[17] G. Eichmann, H. Sanchis-Alepuz, R. Williams, R. Alkofer, and C. S. Fischer, Baryons as relativistic three-quark bound states, Prog. Part. Nucl. Phys. **91,** 1 (2016).

[18] S.-X. Qin and C. D. Roberts, Impressions of the continuum bound state problem in QCD, Chin. Phys. Lett. **37,** 121201 (2020).

[19] G. Eichmann, R. Alkofer, A. Krassnigg, and D. Nicmorus, Nucleon Mass from a Covariant Three-Quark Faddeev Equation, Phys. Rev. Lett. **104,** 201601 (2010).

[20] G. Eichmann, Nucleon electromagnetic form factors from the covariant Faddeev equation, Phys. Rev. D **84,** 014014 (2011).

[21] Q.-W. Wang, S.-X. Qin, C. D. Roberts, and S. M. Schmidt, Proton tensor charges from a Poincaré-covariant Faddeev equation, Phys. Rev. D **98,** 054019 (2018).

[22] S.-X. Qin, C. D. Roberts, and S. M. Schmidt, Spectrum of light- and heavy-baryons, Few Body Syst. **60,** 26 (2019).

[23] S.-X. Qin, L. Chang, Y.-X. Liu, C. D. Roberts, and S. M. Schmidt, Practical corollaries of transverse Ward-Green-Takahashi identities, Phys. Lett. B **722,** 384 (2013).

[24] S.-X. Qin, C. D. Roberts, and S. M. Schmidt, Ward-Green-Takahashi identities and the axial-vector vertex, Phys. Lett. B **733,** 202 (2014).

[25] D. Binosi, L. Chang, S.-X. Qin, J. Papavassiliou, and C. D. Roberts, Symmetry preserving truncations of the gap and Bethe-Salpeter equations, Phys. Rev. D **93,** 096010 (2016).

[26] S.-X. Qin and C. D. Roberts, Resolving the Bethe-Salpeter kernel, Chin. Phys. Lett. **38,** 071201 (2021).

[27] R. T. Cahill, C. D. Roberts, and J. Praschifka, Baryon structure and QCD, Aust. J. Phys. **42,** 129 (1989).

[28] C. J. Burden, R. T. Cahill, and J. Praschifka, Baryon structure and QCD: Nucleon calculations, Aust. J. Phys. **42,** 147 (1989).

[29] H. Reinhardt, Hadronization of quark flavor dynamics, Phys. Lett. B **244,** 316 (1990).

[30] G. V. Efimov, M. A. Ivanov, and V. E. Lyubovitskij, Quark-diquark approximation of the three quark structure of baryons in the quark confinement model, Z. Phys. C **47,** 583 (1990).

[31] M. Y. Barabanov *et al.*, Diquark correlations in hadron physics: Origin, impact and evidence, Prog. Part. Nucl. Phys. **116,** 103835 (2021).

[32] M. Anselmino, E. Predazzi, S. Ekelin, S. Fredriksson, and D. B. Lichtenberg, Diquarks, Rev. Mod. Phys. **65,** 1199 (1993).

[33] I. Aznauryan, V. Burkert, T.-S. Lee, and V. Mokeev, Results from the N* program at JLab, J. Phys. Conf. Ser. **299,** 012008 (2011).

[34] C. Chen, B. El-Bennich, C. D. Roberts, S. M. Schmidt, J. Segovia, and S. Wan, Structure of the nucleon's low-lying excitations, Phys. Rev. D **97,** 034016 (2018).

[35] L. Chang, F. Gao, and C. D. Roberts, Parton distributions of light quarks and antiquarks in the proton, Phys. Lett. B **829,** 137078 (2022).

[36] Y. Lu, L. Chang, K. Raya, C. D. Roberts, and J. Rodríguez-Quintero, Proton and pion distribution functions in counterpoint, Phys. Lett. B **830,** 137130 (2022).

[37] D. Abrams *et al.*, Measurement of the Nucleon F_2^n/F_2^p Structure Function Ratio by the Jefferson Lab MARATHON Tritium/Helium-3 Deep Inelastic Scattering Experiment, Phys. Rev. Lett. **128,** 132003 (2022).

[38] Z.-F. Cui, F. Gao, D. Binosi, L. Chang, C. D. Roberts, and S. M. Schmidt, Valence quark ratio in the proton, Chin. Phys. Lett. **39,** 041401 (2022).

[39] M. Oettel, G. Hellstern, R. Alkofer, and H. Reinhardt, Octet and decuplet baryons in a covariant and confining diquark—quark model, Phys. Rev. C **58,** 2459 (1998).

[40] I. C. Cloet, A. Krassnigg, and C. D. Roberts, Dynamics, symmetries and hadron properties, in *Proceedings of the 11th International Conference on Meson-Nucleon Physics and the Structure of the Nucleon (MENU 2007)*, edited by H. Machner and S. Krewald (2007), p. 125, https://ui.adsabs.harvard.edu/abs/2007arXiv0710.5746C/abstract.

[41] T. Hilger, M. Gomez-Rocha, and A. Krassnigg, Light-quarkonium spectra and orbital-angular-momentum decomposition in a Bethe–Salpeter-equation approach, Eur. Phys. J. C **77,** 625 (2017).

[42] S. Weinberg, Precise Relations between the Spectra of Vector and Axial Vector Mesons, Phys. Rev. Lett. **18,** 507 (1967).

[43] L. Chang and C. D. Roberts, Tracing masses of ground-state light-quark mesons, Phys. Rev. C **85,** 052201(R) (2012).

[44] R. Williams, C. S. Fischer, and W. Heupel, Light mesons in QCD and unquenching effects from the 3PI effective action, Phys. Rev. D **93,** 034026 (2016).

[45] C. D. Roberts, Empirical consequences of emergent mass, Symmetry **12,** 1468 (2020).

[46] C. D. Roberts, D. G. Richards, T. Horn, and L. Chang, Insights into the emergence of mass from studies of pion and kaon structure, Prog. Part. Nucl. Phys. **120,** 103883 (2021).

[47] A. C. Aguilar, M. N. Ferreira, and J. Papavassiliou, Exploring smoking-gun signals of the Schwinger mechanism in QCD, Phys. Rev. D **105,** 014030 (2022).

[48] D. Binosi, Emergent hadron mass in strong dynamics, Few Body Syst. **63,** 42 (2022).

[49] T. Horn and C. D. Roberts, The pion: An enigma within the Standard Model, J. Phys. G **43,** 073001 (2016).

[50] P.-L. Yin, Z.-F. Cui, C. D. Roberts, and J. Segovia, Masses of positive- and negative-parity hadron ground-states, including those with heavy quarks, Eur. Phys. J. C **81,** 327 (2021).

[51] R. Alkofer, A. Höll, M. Kloker, A. Krassnigg, and C. D. Roberts, On nucleon electromagnetic form-factors, Few Body Syst. **37,** 1 (2005).

[52] H. L. L. Roberts, L. Chang, I. C. Cloet, and C. D. Roberts, Masses of ground and excited-state hadrons, Few Body Syst. **51,** 1 (2011).

[53] J. Segovia, I. C. Cloet, C. D. Roberts, and S. M. Schmidt, Nucleon and Δ elastic and transition form factors, Few Body Syst. **55,** 1185 (2014).

[54] L. X. Gutiérrez-Guerrero, G. Paredes-Torres, and A. Bashir, Mesons and baryons: Parity partners, Phys. Rev. D **104,** 094013 (2021).

[55] R. B. Lehoucq, D. C. Sorensen, and C. Yang, *ARPACK Users' Guide: Solution of Large-Scale Eigenvalue Problems with Implicitly Restarted Arnoldi Methods* (Society for Industrial and Applied Mathematics, 1998), p. 142.

[56] Y. Qiu, Sparse Eigenvalue Computation Toolkit as a Redesigned ARPACK (SPECTRA) (2021), https://spectralib.org/index.html.

[57] B. Julia-Diaz, T. S. H. Lee, A. Matsuyama, and T. Sato, Dynamical coupled-channel model of pi N scattering in the $W \leq 2$-GeV nucleon resonance region, Phys. Rev. C **76,** 065201 (2007).

[58] N. Suzuki, B. Julia-Diaz, H. Kamano, T. S. H. Lee, A. Matsuyama, and T. Sato, Disentangling the Dynamical Origin of P-11 Nucleon Resonances, Phys. Rev. Lett. **104,** 042302 (2010).

[59] D. Rönchen, M. Döring, F. Huang, H. Haberzettl, J. Haidenbauer, C. Hanhart, S. Krewald, U. G. Meissner, and K. Nakayama, Coupled-channel dynamics in the reactions $\pi N \to \pi N$, ηN, $K\Lambda$, $K\Sigma$, Eur. Phys. J. A **49,** 44 (2013).

[60] H. Kamano, S. X. Nakamura, T. S. H. Lee, and T. Sato, Nucleon resonances within a dynamical coupled-channels model of πN and γN reactions, Phys. Rev. C **88,** 035209 (2013).

[61] G. Eichmann, R. Alkofer, I. C. Cloet, A. Krassnigg, and C. D. Roberts, Perspective on rainbow-ladder truncation, Phys. Rev. C **77,** 042202(R) (2008).

[62] G. Eichmann, I. C. Cloet, R. Alkofer, A. Krassnigg, and C. D. Roberts, Toward unifying the description of meson and baryon properties, Phys. Rev. C **79,** 012202(R) (2009).

[63] A. Höll, A. Krassnigg, and C. D. Roberts, Pseudoscalar meson radial excitations, Phys. Rev. C **70,** 042203(R) (2004).

[64] B.-L. Li, L. Chang, F. Gao, C. D. Roberts, S. M. Schmidt, and H.-S. Zong, Distribution amplitudes of radially-excited π and K mesons, Phys. Rev. D **93,** 114033 (2016).

[65] S.-X. Qin, L. Chang, Y.-x. Liu, C. D. Roberts, and D. J. Wilson, Investigation of rainbow-ladder truncation for excited and exotic mesons, Phys. Rev. C **85,** 035202 (2012).

[66] G. Eichmann and D. Nicmorus, Nucleon to Delta electromagnetic transition in the Dyson-Schwinger approach, Phys. Rev. D **85**, 093004 (2012).

[67] Y. Lu, C. Chen, Z.-F. Cui, C. D. Roberts, S. M. Schmidt, J. Segovia, and H. S. Zong, Transition form factors: $\gamma^* + p \to \Delta(1232)$, $\Delta(1600)$, Phys. Rev. D **100**, 034001 (2019).

[68] G. Eichmann, C. S. Fischer, and H. Sanchis-Alepuz, Light baryons and their excitations, Phys. Rev. D **94**, 094033 (2016).

[69] S.-X. Qin, C. D. Roberts, and S. M. Schmidt, Poincaré-covariant analysis of heavy-quark baryons, Phys. Rev. D **97**, 114017 (2018).

[70] V. I. Mokeev (private communication).

[71] V. I. Mokeev, Insight into EHM from results on electro-excitation of $\Delta(1600)3/2^+$ resonance, in *Perceiving the Emergence of Hadron Mass through AMBER @ CERN—VII* (2022), https://indico.cern.ch/event/1145356/contributions/4850020/.

[72] V. D. Burkert, R. De Vita, M. Battaglieri, M. Ripani, and V. Mokeev, Single quark transition model analysis of electromagnetic nucleon resonance transitions in the [70,1-] super-multiplet, Phys. Rev. C **67**, 035204 (2003).

[73] M. Dugger *et al.*, π^+ photoproduction on the proton for photon energies from 0.725 to 2.875-GeV, Phys. Rev. C **79**, 065206 (2009).

[74] V. I. Mokeev and I. G. Aznauryan, Studies of N^* structure from the CLAS meson electroproduction data, Int. J. Mod. Phys. Conf. Ser. **26**, 1460080 (2014).

[75] E. L. Isupov *et al.*, Measurements of $ep \to e'\pi^+\pi^- p'$ cross sections with CLAS at 1.40 Gev $< W <$ 2.0 GeV and 2.0 GeV$^2 < Q^2 <$ 5.0 GeV^2, Phys. Rev. C **96**, 025209 (2017).

[76] A. Trivedi, Measurement of new observables from the $\pi^+\pi^-$ p electroproduction off the proton, Few Body Syst. **60**, 5 (2019).

[77] Z.-F. Cui, C. Chen, D. Binosi, F. de Soto, C. D. Roberts, J. Rodríguez-Quintero, S. M. Schmidt, and J. Segovia, Nucleon elastic form factors at accessible large spacelike momenta, Phys. Rev. D **102**, 014043 (2020).

[78] C. Chen, Y. Lu, D. Binosi, C. D. Roberts, J. Rodríguez-Quintero, and J. Segovia, Nucleon-to-Roper electromagnetic transition form factors at large Q^2, Phys. Rev. D **99**, 034013 (2019).

[79] C. Chen, C. S. Fischer, C. D. Roberts, and J. Segovia, Form factors of the nucleon axial current, Phys. Lett. B **815**, 136150 (2021).

[80] C. Chen, C. S. Fischer, C. D. Roberts, and J. Segovia, Nucleon axial-vector and pseudoscalar form factors and PCAC relations, Phys. Rev. D **105**, 094022 (2022).

[81] U. Mosel, Neutrino interactions with nucleons and nuclei: Importance for long-baseline experiments, Annu. Rev. Nucl. Part. Sci. **66**, 171 (2016).

[82] O. Oliveira, P. J. Silva, J.-I. Skullerud, and A. Sternbeck, Quark propagator with two flavors of O(a)-improved Wilson fermions, Phys. Rev. D **99**, 094506 (2019).

[83] C. J. Burden, C. D. Roberts, and M. J. Thomson, Electromagnetic form factors of charged and neutral kaons, Phys. Lett. B **371**, 163 (1996).

[84] M. B. Hecht, C. D. Roberts, and S. M. Schmidt, Valence-quark distributions in the pion, Phys. Rev. C **63**, 025213 (2001).